Dynamical resonant neutralization of low-energy Na^+ ions scattered from Au(111), Pd(111), Cu(111), and Cu(110) surfaces

Lei Gao,[1] Yachao Zhu,[1] Yuanqing Shi,[1] Pinyang Liu,[1] Yunqing Xiao,[1] Guopeng Li,[1] Yiran Liu,[1] Vladimir A. Esaulov,[2] Ximeng Chen,[1] Lin Chen,[1,*] and Yanling Guo[1,†]

[1]*School of Nuclear Science and Technology and Key Laboratory of Special Function Materials and Structure Design, Ministry of Education, Lanzhou University, Lanzhou 730000, China*

[2]*Institut des Sciences Moléculaires d'Orsay and CNRS, UMR 8214, Institut des Sciences Moléculaires d'Orsay, Orsay ISMO, Bâtiment 351, Université-Paris Sud, 91405 Orsay, France*

(Received 16 July 2017; published 20 November 2017)

The nonmonotonic energy dependence of the Li^0 fraction on high-work-function surfaces has not been understood so far. To further study this phenomenon, in this work, efficient neutralization of Na^+ ions has been reported on various surfaces, instead of Li^+ ions. The nonmonotonic energy dependence of the Na^0 fraction becomes more and more obvious with the increase of the surface work function. For Cu(111) and Cu(110) at the scattering angle of 7°, the energy dependence of the neutral fraction is still nonmonotonic as compared to the scattering angles of 135° and 53°. For the scattering angle of 53°, the nonmonotonic angle dependence has been observed for these surfaces. The essences of the nonmonotonic angle and energy dependences are the same. The quantum-mechanical calculations reveal that the width and position of the atomic level below the Fermi level at short ion-surface distances are responsible for high neutral fractions at large exit energies, and that the neutral fraction at much smaller exit energies is probably related to the neutralization at large distances. For the exit angle dependence, the competition between neutralization at short and large distances strongly depends on the surface work function. In particular, the neutralization is enhanced by the relatively large parallel velocity.

DOI: 10.1103/PhysRevA.96.052705

I. INTRODUCTION

Charge transfer processes in ion- or atom-surface collisions have been extensively studied both experimentally and theoretically [1–8], since they play important roles not only in the influence on charge states of scattered particles and as a probe of the electronic structure of surfaces, but also in a number of technological applications such as thin-film growth [9], reactive ion etching [10], surface catalysis [11], stimulated desorption [12], secondary-ion mass spectroscopy (SIMS) [13], and low-energy ion scattering (LEIS) [14]. The alkali-metal ions, as a probe, provide a more sensitive and quantitative analysis of surfaces due to their low neutralization probabilities. As a result, understanding the neutralization mechanism of alkali-metal ions on different types of solid surfaces is necessary.

Recent important developments in this field involve alternative materials. The metal-oxide-semiconductor device [$Au/SiO_2/Si(100)$] bombarded by alkali ions was reported to investigate internal hot electrons and the hole excitations at the surface [15,16]. The neutralization of alkali-metal ions scattered from clean and adsorbate-covered surfaces was performed to probe the internal electronic structure of adatoms [17–20]. Experimental studies of alkali-metal ion neutralization on supported Ag and Au clusters were performed [21–23] to illustrate quantum-size effects [24–26]. Recent theory has also addressed the case of electron transfer on ultrathin films and the effect of quantization because of the finite thickness of films [2,27,28]. In the limit of the complete surface coverage by Au(111)-type films, it was observed that efficient neutralization of Li occurs, in spite of a very large (5.4 eV) work function [29]. These curious features are not understandable in the "standard" jellium free-electron gas model. Therefore, a prerequisite for electron transfer on these materials is the knowledge of the characteristic of neutralization of alkali-metal ions on bulk surfaces.

The neutralization of alkali-metal ions on jelliumlike metal surfaces is usually treated in the jellium free-electron gas model of resonant charge transfer (RCT). The ionization levels of alkali-metal ions are generally comparable to typical values of metal work functions. When the atomic level of Na(3*s*) (ionization potential 5.14 eV) is broadened and shifted up by the image potential, remaining below the Fermi level of the surface for large ion-surface distances, the neutralization of Na^+ ions occurs, while for short distances the atomic level shifts above the Fermi level, and then the resonant ionization takes place. As a result, the neutralization probability *decreases monotonically* as the collision velocity increases, because of the shorter electron capture time. This behavior has been confirmed by a number of experimental studies [21,30,31] and supported by the jellium model calculation, mainly for relatively low-work-function surfaces.

In recent years, the neutralization of alkali-metal ions from noble metal surfaces has also been quite actively investigated [32–35]. A series of previous studies of Li^+ neutralization on Cu(100), Cu(111), Au(111), Au(100), Au(110), and Pd(100) surfaces [30,32–34] clearly shows some common characteristics for surfaces with large work function: The neutral fraction is relatively high and tends to first decrease with increasing energy and then increase again. This is not related to the differences in details of the electronic structure of these surfaces, and not understandable in the jellium model calculation. On the theoretical side, recent work [36] has indicated that efficient neutralization of Li^+ scattering on Cu

*chenlin@lzu.edu.cn
†guoyanling@lzu.edu.cn

can occur at small ion-surface distances, because the Li level shifts again below the Fermi level of Cu at distances below 4 a.u. from the first atomic plane. This feature could explain large neutralization for an *atom* receding rapidly from the surface after close approach, as opposed to the standard view of an *ion* receding from the surface. Very recently, additional efforts have been devoted to describing the energy dependence [33,35–38]. However, the question of the nonmonotonic Li^0 fraction dependence remains open.

In order to further understand the nonmonotonic neutralization, we experimentally measured the neutralization probability or fraction of Na^+ ion scattering on Au(111), Pd(111), Cu(111), and Cu(110) surfaces. For Li^+ scattering, in previous studies many high-work-function surfaces have been used [30,32–34], while in the present study we attempt to examine Na^+ instead of Li^+, because the ionization energy of Na ($3s$) (5.14 eV) is smaller than that of Li ($2s$) (5.39 eV). We would intuitively expect to get much less neutralization for Na^+ ion scattering on Au(111) and Pd(111) since the ionization energy of Na($3s$) is significantly smaller than the work function of these two surfaces. As a comparison with that, we have also measured the neutral fractions from Cu(111) and Cu(110) surfaces with relatively smaller work function ($W_{Cu(111)} = 4.95$ eV, $W_{Cu(110)} = 4.49$ eV). In this work, a simple theoretical model has also been presented, examining the influence of the atomic level of the projectile on neutral fraction at short ion-surface distances. Moreover, the parallel velocity effect has been taken into account. The comparison between our experimental results and theoretical calculations allows us to improve the understanding of the dynamical electron transfer characteristics of these exciting collisional systems.

II. EXPERIMENT

The experiments were performed in an ion-scattering apparatus, shown schematically in Fig. 1. The main ultrahigh-vacuum (UHV) chamber has a diameter of 60 cm and is equipped for ion-scattering spectroscopy (ISS) and time-of-flight scattering and recoiling spectroscopy (TOF-SARS). It has homemade Na^+ and Ar^+ ion guns, an electron gun, an evaporator, and a quartz crystal microbalance (QCM). The base pressure in the chamber is about 2×10^{-8} Pa attained with the help of UHV turbomolecular and ion pumps. Na^+ ions, with incident energies of 0.16–5 keV, are collimated to the beam size of $1 \times 3\,mm^2$ and directed to the sample. The sample was placed on a precision manipulator in the chamber. Adjusting the manipulator, we can change the incident (exit) angle measured with respect to the surface plane. In this work, scattering angles were fixed at 135°, 53°, and 7°, respectively. The sample azimuthal orientation was set arbitrarily.

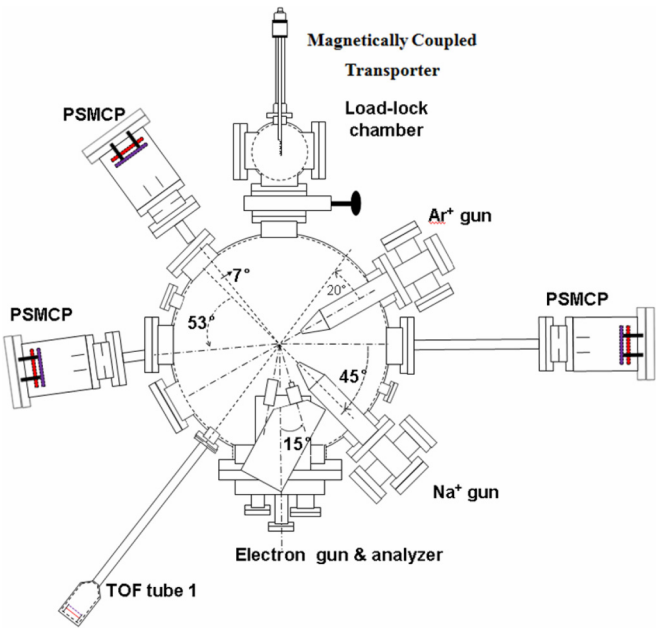

FIG. 1. Schematic diagram of the experimental setup.

The reflected particles from the surface passed through the two post-target separated slits to avoid scattering on the wall of the flight tube. The charge states of scattered particles were then analyzed by a parallel-plate electrostatic analyzer. At the end of the flight tube, charge-state separated particles were recorded by a one-dimensional position sensitive microchannel plate (PSMCP) detector [8,39]. The neutral fraction is defined as $N(Na^0)/N(Na^0 + Na^+)$ where $N(Na^0)$ and $N(Na^+)$ are the number of scattered particles corresponding to two separated peaks recorded by the PSMCP detector. This can be measured in a continuous-beam mode or pulsed-beam mode using the TOF technique. As previously studied in Li^+ neutralization [33], we did not observe significant differences between the neutral fractions measured by these two beam modes. The PSMCP detector consists of two 56-mm-diameter microchannel plates (MCPs) stacked in a chevron configuration and mounted above a $56 \times 11\,mm^2$ strip-type resistive anode. The face of the first MCP is at ground potential and the resistive anode is kept at 2200 V at which the measured count rate becomes independent of pulse height. The detector efficiency for particles with different charge states is assumed to be identical at fixed energies [40–42]. A multiparameter acquisition system [43] was used for data collection.

In situ preparation of the Au(111), Pd(111), Cu(111), and Cu(110) surfaces consisted of many cycles of 3-keV Ar^+ sputtering with a beam density of $2.0\,\mu A/cm^2$ (30 min) and subsequent annealing at about 770 K (15 min) using electron bombardment. During sputtering, the sample was periodically moved along the direction parallel and perpendicular to the beam to ensure that the entire surface was exposed to the beam uniformly. Surface cleanliness was then verified by TOF-SARS using 3-keV Ar^+ ions scattering on the sample with a scattering angle of 20° and incident angles of 5° and 10° [44,45].

One of the main concerns in experiments of this type is the possibility of Na implantation which would change the surface work function. As an example, Fig. 2 shows TOF spectra of Au(111) by TOF-SARS. There are two small peaks on the right-hand side of the big peak of scattered argon, corresponding to the recoil Na and impurity S particles (see the inset). The relative intensity of Na (S) is defined as the ratio of the recoil Na (S) intensity to the scattered Ar intensity. About 0.8% Na is implanted into the sample after a long measurement time using Na^+ ions (see the black line). The recoil S particles come from the bulk impurity. The annealing process enhances the segregation of S to the surface. This segregation can be

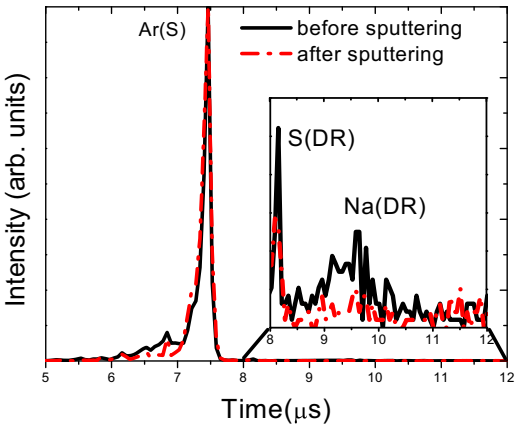

FIG. 2. TOF spectra for 3-keV Ar^+ ions scattering on Au(111) with an incident angle of 10° and a scattering angle of 20°. Na(DR) and S(DR) represent the recoil Na and S particles from the surface, respectively. Ar(S) denotes the scattered Ar particles. The recoil intensities of adsorbates such as Na and S are significantly reduced after many cycles of sputtering and annealing.

removed continuously by ion bombardment. After many cycles of preparing the surface with care, the amount of S impurities approximately decreases from 0.4% down to 0.3%, and Na is below 0.3% close to the background level. It is regarded as a clean surface. Furthermore, cross checks of the surface cleanliness are made at the beginning, in the middle, and at the end of a series of measurements.

III. RESULTS

During the measurements, we found that no recoil Au and Pd particles are observed in the TOF spectra for energetic Na ion scattering on Au(111) and Pd(111) surfaces, respectively, as shown in Fig. 3. In contrast, for Cu(111) and Cu(110), we observed some recoil Cu particles, particularly for large incident energies and around the specular scattering geometry. Thus we have corrected the neutral fractions via the TOF spectra for Cu(111) and Cu(110) surfaces in the following figures.

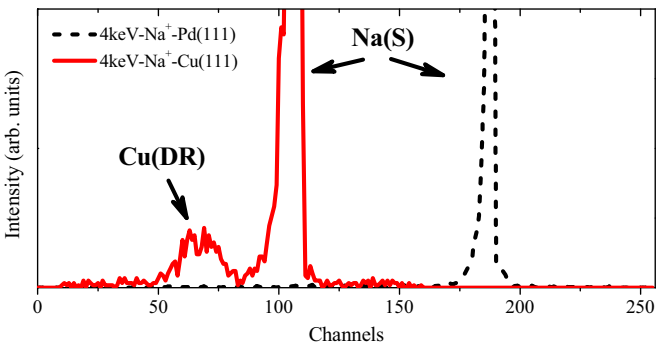

FIG. 3. TOF spectra for 4-keV Na^+ ions scattering on Pd(111) and Cu(110) surfaces with an incident angle of 25° and a scattering angle of 53°. Na(S) and Cu(DR) represent the scattered Na and recoil Cu particles from the surface, respectively.

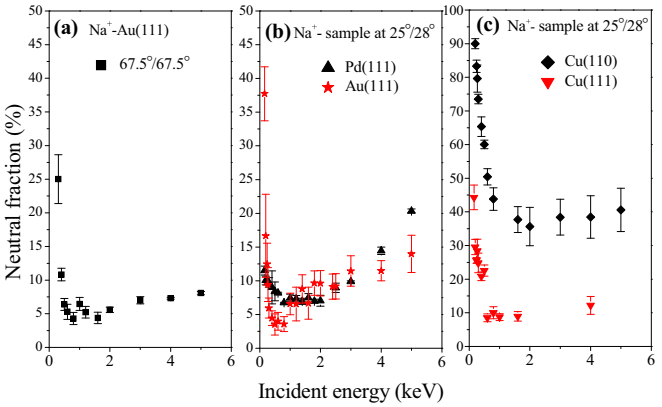

FIG. 4. (a) Neutral fractions obtained on a Au(111) surface as a function of incident energy of Na^+ at a scattering angle of 135°. (■) corresponds to an incident angle of 67.5° and an exit angle of 67.5°. (b) Neutral fractions obtained on Pd(111) (▲) and Au(111) (★) surfaces for a scattering angle of 53° with an incident angle of 25° and an exit angle of 28°. (c) Neutral fractions obtained on Cu(110) (◆) and Cu(111) (▼) surfaces for a scattering angle of 53° with an incident angle of 25° and an exit angle of 28°.

We measured neutral fractions for 0.16–5-keV Na^+ ions scattering on Au(111), Pd(111), Cu(111), and Cu(110) surfaces as a function of incident energy for a random scattering azimuth. For the scattering angle of 135°, Fig. 4(a) shows neutral fractions for Na^+ in specular scattering on Au(111) with an incident angle of 67.5°. We find a fairly large neutral fraction of about 2.5%–25%. It is surprising that efficient neutralization is still observed for Na with a lower ionization energy (5.14 eV) as compared to Li (5.39 eV) on a surface with the large work function of 5.4 eV. The neutral fraction first decreases with the increase of incident energy, and then increases as incident energy increases. At low energies a significantly higher neutral fraction is observed. This nonmonotonic incident energy dependence has also been observed in the previous studies on the neutralization of Li^+ ions scattering on Au(111) [32] and Cu(111) [32,37], and Au(110) and Pd(100) surfaces [33] in the lower incident energy range of <2 keV.

For a scattering angle of 53° with an exit angle of 28°, in Figs. 4(b) and 4(c), the neutral fractions for Au(111), Pd(111), Cu(111), and Cu(110) surfaces are displayed together for comparison. For Au(111), the neutral fraction has a similar trend and magnitude to that shown in Fig. 4(a). For Cu(111), the curve trend is also similar and the neutral fraction is slightly larger than that of Au(111). It indicates that the different scattering angles of 135° and 53° have no influence on the shape of the energy dependence of the neutral fraction.

For Pd(111) and Cu(110) surfaces, the neutral fractions decrease monotonically when the incident energy is less than 2 keV, and the trends are similar to the results measured for low-work-function surfaces like Ag(111) [32], Cu(001) [37], and Ag(001) [46] at incident energies less than 2 keV. While for the incident energy more than 2 keV, the neutral fraction for Cu(110) does not continuously decrease and it seems to increase slightly. For Pd(111) the neutral fraction increases significantly, at incident energies between 2 and 5 keV, from

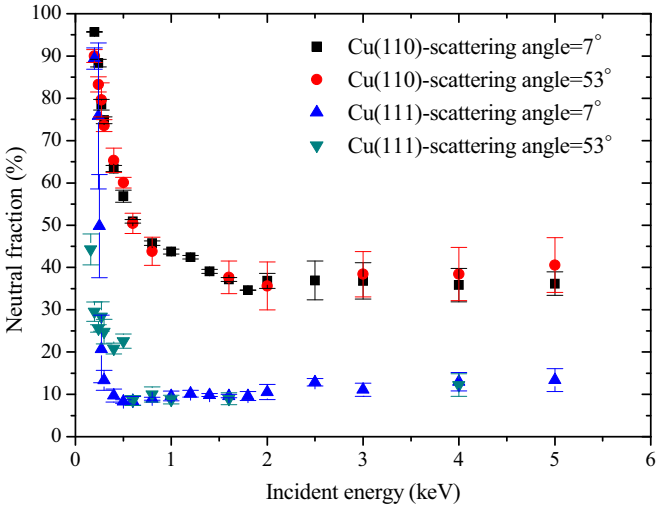

FIG. 5. Neutral fractions obtained in scattering on Cu(111) and Cu(110) surfaces as a function of incident energy of Na^+ for scattering angles of 53° (an incident angle of 25° and an exit angle of 28°) and 7° (in specular scattering). (■) and (●) correspond to scattering angles of 7° and 53° on Cu(110), respectively; (▲) and (▼) correspond to scattering angles of 7° and 53° on Cu(111), respectively.

about 10% up to 20%. In addition, the neutral fraction of Pd(111) is similar to that of Li^+ in specular scattering on Pd(100) at a scattering angle of 83° [33].

It is interesting that the neutral fraction of Na^+ scattering on Cu(111) at a scattering angle of 53° is nearly the same as that at a scattering angle of 7° (in specular scattering) when the incident energy is larger than 0.5 keV, as shown in Fig. 5, but below 0.5 keV, the neutral fraction for the scattering angle of 7° increases faster than that for the scattering angle of 53° with the decrease of incident energy. For Cu(110), the neutral fractions measured at two scattering angles are also similar to each other. It indicates again that the shape of the energy dependence does not change for different scattering angles investigated.

We display in Fig. 6 the exit-angle-dependent neutral fractions for Na^+ scattering on Au(111), Cu(111), Pd(111), and Cu(110) surfaces at the 53° scattering angle. The non-monotonic behavior of the neutral fractions is qualitatively similar to the Li^+ neutralization results on Au(110) and Pd(100) at the 83° scattering angle [33]. In particular, the exit angle corresponding to the minimum of neutral fraction decreases from ∼40° to ∼22° with the increase of work function. As an example, in Fig. 6(d) we present the neutral fractions for 0.4-, 0.6-, 0.8-, and 1.6-keV Na^+ ions. As the incident energy increases, the neutral fraction decreases and its minimum region becomes broader for Cu(110) [Fig. 6(d)] with the lowest work function (4.49 eV). The trend of the neutral fraction of 1.6-keV Na^+ ions is similar to other surfaces as shown in Figs. 6(a)–6(c). It indicates that the nonmonotonic exit angle dependence could be a common feature for surfaces, whatever the work function.

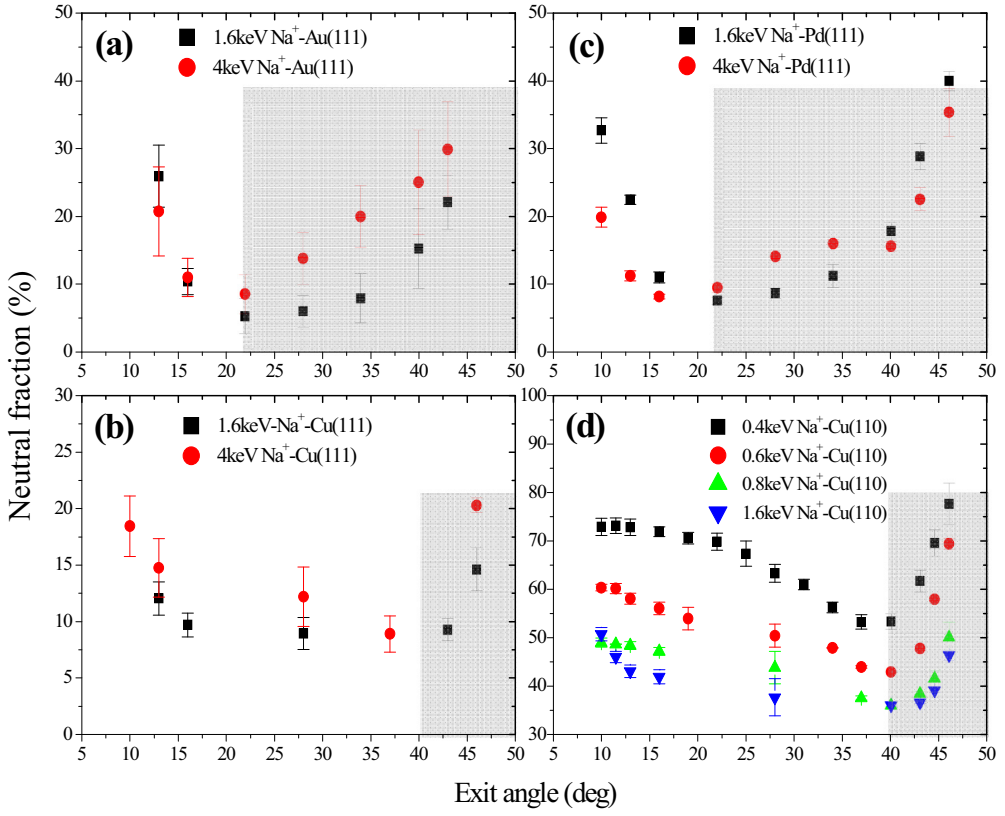

FIG. 6. Neutral fractions as a function of exit angle for 1.6-keV (■) and 4-keV (●) Na^+ scattering on (a) Au(111), (b) Cu(111), (c) Pd(111) surfaces with a scattering angle of 53°. (d) Neutral fractions for Cu(110) in collisions with 0.4-, 0.6-, 0.8-, and 1.6-keV Na^+ at a scattering angle of 53°, respectively. The gray area represents the increasing neutral fractions at large exit angles.

IV. DISCUSSION

In the experiment, we observe dynamical neutralization of Na^+ ions scattering on various surfaces with different work function values. The nonmonotonic behavior has been observed in the incident energy and exit angle dependences. The efficient neutralization of Na^+ on Au(111) and Pd(111) is surprising, because its ionization energy level is above the Fermi level of these surfaces. For Pd(111) and Cu(110), the neutral fraction first monotonically decreases (<2 keV), and then increases at incident energies between 2 and 5 keV. For Cu(111) and Cu(110), the neutral fraction at a scattering angle of 7° is nearly the same as that at 53°. The angle dependences of the neutral fraction are still nonmonotonic for these four surfaces.

In the following, we will focus on the understanding of the nonmonotonic energy and angle dependences of neutral fraction on various surfaces and modify the Brako-Newns (BN) model in two aspects: (1) the projectile energy level and width near the surface; (2) the parallel velocity effect.

A. Width and position of atomic level

As we know, the simple jellium model using the rate equation can reproduce well the experimental results of Li^+ neutralization on Cu(100) [30] and Ag(100) [31] where the neutral fraction monotonically decreases with incident energy, but it fails to describe the neutralization of Li^+ ion scattering on Au(111) and Cu(111) [32], Au(110) and Pd(100) [33], and Au(100) [34], and the neutralization of Na^+ ion on Cu(001) [47], in which the nonmonotonic neutral fractions have been observed.

In the previous work [33], we have calculated the number of Li valence electrons as a function of the atom distance to the surface and embedded it in the rate equation with an adjustable free parameter. This static charge evolution comes from the first-principle calculation of density functional theory (DFT). On the other hand, there are state-of-the-art theories developed by Gauyacq and Borisov and co-workers [48,49] and Onufriev and Marston [50], as well as by Goldberg and co-workers [37]. From the view of experimentalists, one prefers to roughly estimate the neutral fraction using a simple model with an intuitive physical picture, taking a small amount of computing time. The BN model is easy to handle [47,51], which recently has been used to understand the efficient neutralization of Li^+ and Na^+ ions scattered from metal surfaces [52].

The BN model is one of the forms of the spinless one-level Newns-Anderson Hamiltonian and allows for a determination of the occupancy of the projectile atomic level after scattering from the surface. The details of BN model can be found elsewhere [51]. According to the BN model the occupancy of the atomic state $n_a(t)$ as a function of time t is given by

$$n_a(t) = n_a(t_0)\exp\left[-2\int_{t_0}^{t}\Delta(t')dt'\right] + \frac{1}{\pi}\int d\varepsilon f(\varepsilon,T) \times \left|\int_{t_0}^{t}\sqrt{\Delta(t')}\exp\left(-i\varepsilon t' - \int_{t'}^{t}[i\varepsilon_a(t'') + \Delta(t'')]dt''\right)dt'\right|^2, \quad (1)$$

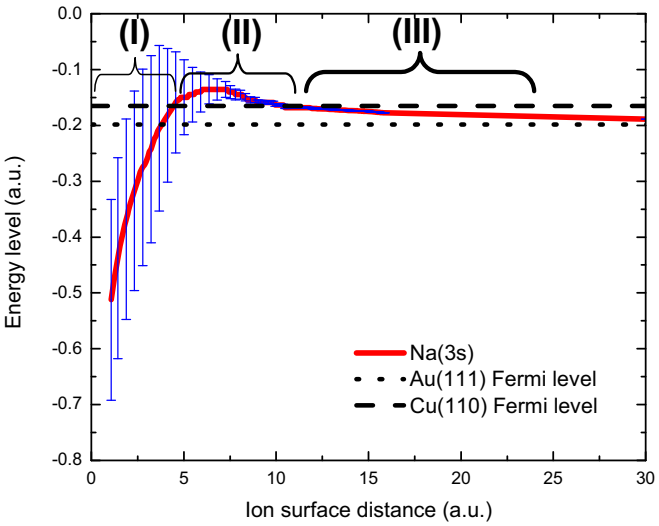

FIG. 7. The Na(3s) energy-level position and width as a function of ion-surface distance. The zero of the energy scale is set at the vacuum level. The red line represents the downshift of the energy level with decreasing the ion-surface distance and the energy width is given by error bars; the black dotted and dashed lines represent the Fermi level of Au(111) and Cu(110), respectively. The Na(3s) energy-level behavior can be divided into three regions with respect to the Fermi level of Cu(110): (I) below the Fermi level at short distances, (II) above the Fermi level, and (III) below the Fermi level again.

where $f(\varepsilon,T) = \frac{1}{1+\exp[(\varepsilon-\mu)/k_BT]}$ is the Fermi distribution, and $\mu = 5.51$ eV is the chemical potential of gold, with 7.00 and 7.69 eV for copper and palladium, respectively. k_B is the Boltzmann constant, and temperature $T = 300$ K. The half width of the atomic resonance is given by [47]

$$\Delta(t) = \frac{\Delta_0}{\left[e^{4\alpha z(t)} + \left(\frac{\Delta_0}{\Delta_{\rm sat}}\right)^4\right]^{1/4}}. \quad (2)$$

For $z(t) \to 0$, $\Delta(t) \to \Delta_{\rm sat}$ provided that $\Delta_0 \gg \Delta_{\rm sat}$ which is typically true. For $\Delta_{\rm sat} \to \infty$, the simple exponential form $\Delta(t) = \Delta_0 e^{-\alpha z(t)}$ is obtained. In this work, $\Delta_{\rm sat} = 0.18$ a.u. [37], $\Delta_0 = 0.83$ a.u., $\alpha = 0.70$ [53], and the related energy width is given by error bars as shown in Fig. 7.

In Eq. (1), the first term is the memory term and represents the decay of the initial filled level into the unoccupied metal states. $n_a(t_0)$ is the initial occupation. The second term describes the creation and annihilation of charge on the atom along its trajectory. In Eq. (2), we have considered that the energy-level width is finite at short ion-surface distances.

Normally, the energy level $\varepsilon_a(t)$ of the atomic state of the positive projectile shifts upward as the ion-surface distance decreases. In the scattering of Li^+ on Cu(100) and Cu(111) surfaces [36], and on a highly oriented pyrolytic graphite (HOPG) surface [54], Goldberg and co-workers theoretically found the downshift of the ground-state energy level of Li(2s) close to the surface which is the result from the interaction of a Li projectile with all the surface atoms of the solid along its trajectory. We assume that the shape of the energy level of Na is similar to that of Li [37], although we have not found the exact expression in the literature at present. Following the

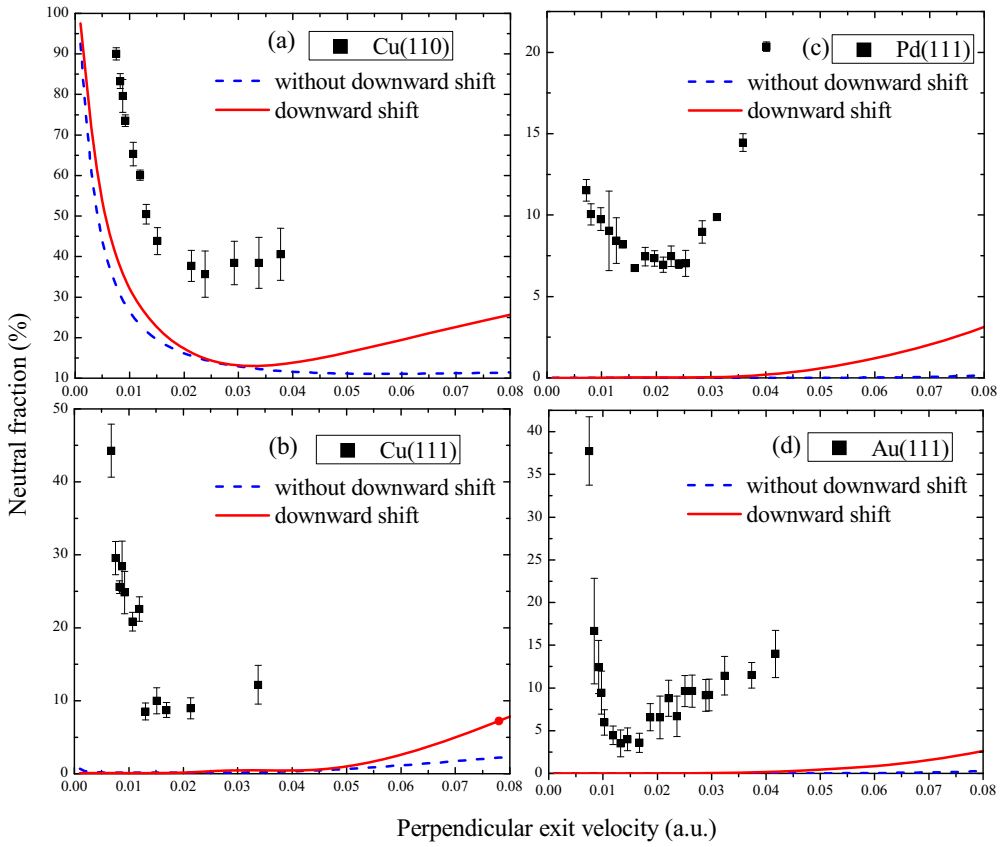

FIG. 8. Neutral fractions obtained in scattering on Cu(111), Cu(110), Pd(111), and Au(111) as a function of perpendicular exit velocity of Na^+ ions, corresponding to a scattering angle of 53°, and an exit angle of 28°. The solid and dashed lines are calculated results with and without the energy-level downward shift with the decrease of ion-surface distances, respectively.

shape of the Li level, the fitting expression is given by

$$\varepsilon_a(t) = \begin{cases} A_0 + A_1 z(t) + A_2 z(t)^2 + \cdots + A_6 z(t)^6, & z(t) \leqslant 7.44\,\text{a.u.} \\ -0.232\,63 + \frac{1}{4[z(t)-3.3669]}, & z(t) > 7.44\,\text{a.u.} \end{cases}, \tag{3}$$

where $A_0 = -0.311\,24$, $A_1 = 0.240\,12$, $A_2 = -0.027\,98$, $A_3 = -9.663\,86 \times 10^{-5}$, $A_4 = 2.245\,11 \times 10^{-4}$, $A_5 = -1.466\,74 \times 10^{-5}$, and $A_6 = 2.949\,08 \times 10^{-7}$, $z(t)$ is the ion-surface separation measured from the real surface.

In Fig. 7, Eq. (3) describes the downward shift of the atomic level of Na, which simply shifts up 0.25 eV (the binding energy difference between Na and Li) with respect to the atomic level of Li. For Cu(110), the energy level of Na(3*s*) has been divided into three parts. Region I corresponds to the electron capture region where the atomic level is below the Fermi level of Cu(110), region II is associated with electron loss, and region III is associated with electron capture again at large distances, while for Au(111) with high work function, there are only regions I and II.

In Fig. 8, we calculate neutral fractions of Na^+ scattered from these surfaces, using the lifetime and energy of the Na(3*s*) resonance calculated by Nordlander and Tully [53], and Borisov *et al.* [55] (not shown here). The exit velocity is calculated with the binary collision model from the interaction energy of the dimer projectile-metal atom system. For Cu(111), the calculated neutral fraction using Nordlander's width is nearly the same as Borisov's. For Cu(110), Pd(111), and Au(111) surfaces, it seems that the calculation using Nordlander's width is closer to the experimental data. The calculations without the downward shift of energy level have been displayed in the figure for comparison. For low perpendicular exit velocity, the position of atomic energy level at short distances (region I) has no significant influence on the neutral fraction, but at relatively high velocities the effect of the downward shift of the atomic level on the neutral fraction is significant. It indicates that at relatively high velocities neutral atoms coming from neutralization at short distances (region I) survive along the outgoing trajectory due to the short interaction time. Note that, in the energy range investigated, we find that the initial occupation $n_a(t_0) = 1$ or 0 has no influence on the final neutral fraction, which indicates the memory of the initial charge state is lost.

Considering the downward shift of the atomic level of Na below the Fermi level at short distances, the calculated neutral fraction for Cu(110) presents a nonmonotonic velocity dependence. The neutral Na atoms are formed in region I and become positive ions in region II as they move away

from the surface, as shown in Fig. 7. The low exit velocities, corresponding to the long interaction time, could cause the neutral atoms formed in region I to completely become positive ions in region II. In contrast, the high exit velocity could cause the survival of a fraction of the neutralized ions in region II. These resulting positive ions are efficiently neutralized again in region III where the low neutralization is expected for the short interaction time. As a result, for low exit velocities, the neutralization in region III determines the final neutral fraction, so that the calculated neutral fraction for Cu(110) monotonically decreases with increasing exit velocity. In contrast, for high perpendicular exit velocities, what happens close to the surface becomes more important. The neutralized atoms survive in region II and dominate the final neutral fraction, so that the interaction time for reionization decreases, resulting in the increment of the survival probability of neutral atoms for high exit velocities.

As opposed to the case of Cu(110), this model does not reproduce well the nonmonotonic velocity dependence of neutral fraction on Cu(111), Au(111), and Pd(111) surfaces (see Fig. 8), although we consider the position and width of atomic level at short ion-surface distances. Goldberg and co-workers [36,37,54] reported that theoretical calculations can satisfactorily describe the trend of neutral fraction for Li^+ scattering on Cu(100) and Cu(111) at high exit energies, but fail at low exit energies, which is similar to our case. At a projectile-surface distance of about 14 (8) a.u. for Cu(111) [Cu(001)], the projectile energy level crosses below the Fermi level which makes the electron capture process possible; however, electron capture would be impossible due to a negligible energy width at these distances. In a recent paper [37], the coupling interaction of a Li-Cu system that requires the inclusion of more surface atoms adds a slight contribution to the energy-level width and makes electron capture viable at such large distances (see Fig. 9 in Ref. [37]).

In Fig. 7, the energy level of Na($3s$) follows the behavior of Li($2s$) [36,37] (see the red line). For Au(111), efficient neutralization occurs at short distances (region I), while electron capture would be impossible at large distances (region II) due to a negligible energy width. Thus the final neutral fraction is mainly determined by the interaction time near the surface. At low perpendicular exit velocities, departing from the surface, the formed neutral atoms spend more time above the Fermi level of Au(111) and completely lose the electron and finally become positive ions. In contrast, at high perpendicular exit velocities, we can observe a large survival probability of neutral atoms, as shown in Fig. 8. Neutralization on Pd(111) and Cu(111) is the same as on Au(111).

It should be pointed out that the reionization of Na atoms could possibly contribute to the reduction of neutralization at high incident energies. The reionization of Na atoms will lead to loss of more kinematic energies. In the time-of-flight spectra of 2-keV Na^+ scattering from $Bi_2Sr_2CaCu_2O_{8+\delta}$ at a scattering angle of 150°, a broad shoulder at longer flight times corresponding to neutral atoms losing more energies has been observed [56]. This structure has also been previously observed for 3-keV Na^+ scattering from a CeO_2(100) surface at a scattering angle of 150° [57]. It indicates that, even if the projectile is reionized, it suffers neutralization again and contributes to the broad background spectra of neutral atoms. In the scattering angle of 95°, for 3-keV Na^+ scattering on Au(111), we have not found an obvious shoulder structure (not shown here), which is similar to that shown in Refs. [20,23]. In Fig. 5, in this work, for the scattering angle of 7°, reionization of Na does not take place due to very large impact parameters. The impact parameter is the perpendicular distance between the path of a projectile and the center of a potential field created by the target that the projectile is approaching. Moreover, the neutral faction monotonically increases with the increase of incident energy, and has no trend of decrease at high energies. Therefore, to some extent, in our case reionization plays a less important role in the energy dependence of neutral fractions.

B. Parallel velocity effect

In Fig. 6 for Na^+ scattering on Au(111), large exit angles correspond to large perpendicular exit velocities where the initially formed neutral atom spends a shorter time near the surface and undergoes less electron loss. Nevertheless, at small exit angles, the increased neutral fraction cannot be qualitatively understood. On the other hand, for the energy dependence a big difference between calculation and experiment has been observed. It may be related to the kinetically parallel velocity effect.

The parallel velocity effect has been well studied in ion-surface scattering at grazing incidence angles where Winters [58] and Borisov and co-workers [59,60] develop the nonperturbative coupled angular mode model. Combining the rate equation, they give quantitative correspondence to experimental data for grazing scattering. Here we simply use the Doppler-Fermi-Dirac distribution function instead of the Fermi function $f(\varepsilon,T)$, which is given by [58]

$$f_{k+Q} = \begin{cases} 1 & , \ k \leqslant k_F - Q \\ \frac{k_F^2-(k-Q)^2}{4kQ}, & k_F - Q < k < k_F + Q \\ 0 & , \ k \geqslant k_F + Q \end{cases}, \qquad (4)$$

where k_F and k are the Fermi momentum and momentum of metal electrons, and Q is the parallel velocity of the scattered particles.

Considering the downward shift of the atomic level and the parallel velocity effect, we have calculated the neutral fractions as a function of perpendicular exit velocity using the modified BN model, as shown in Fig. 9. The results without the parallel velocity effect have also been displayed in the figure for comparison. For a fixed exit angle, high perpendicular exit velocity corresponds to high parallel velocity. It is observed that the parallel velocity effect is significant at relatively high exit velocities and disappears at low perpendicular exit velocities [see Fig. 9(a)]. At high perpendicular exit velocities, the increased neutral fraction is due to the parallel velocity effect which enhances the effective overlap between the resonance shell and the Fermi sphere in the vicinity of the crossing point between regions I and II.

The nonmonotonic angle and exit velocity dependences are explained in the same physical picture. In Fig. 6, the gray areas present the neutralization taking place in region I (short distances). At large exit angles, for a given incident

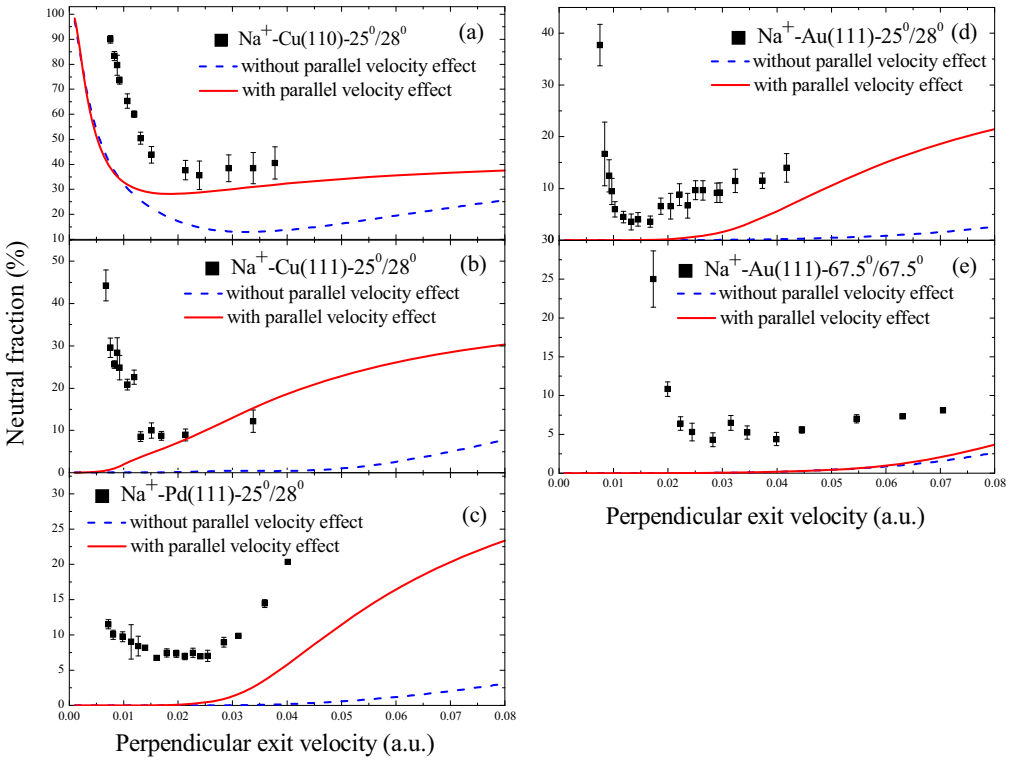

FIG. 9. The calculated neutral fractions obtained in scattering on Cu(110), Cu(111), Pd(111), Au(111) as a function of perpendicular exit velocity for fixed scattering angles of 53° and 135° as labeled. In (a)–(d) for the scattering angle of 53°, the incident angle is 25° and the exit angle is 28°. In (e) for the scattering angle of 135°, the incident angle is 67.5° and the exit angle is 67.5°. The experimental data are from Fig. 4. The lines are calculated results with and without parallel velocity effects, respectively.

energy, the formed neutral atoms (in region I) will survive in region II when departing from the surface due to the short interaction time, which is similar to the case of high exit velocity. As a consequence, the survival of neutral atoms decreases with the decrease of exit angle. The calculation without the parallel velocity effect supports this as shown in Figs. 10(a)–10(c) for Au(111), Pd(111), and Cu(111), although the calculated results are much smaller than the data. In contrast, for Cu(110) in Fig. 10(d), the calculation without the parallel velocity effect fails at large exit angles, and it monotonically decreases with increasing exit angle. It indicates that in the calculation the contribution of the neutralization at short distances has been hidden by that at large distances, but the neutralization at short distances has still been experimentally observed for Cu(110), which indicates that exit angle is an appropriate parameter to study the short-distance interaction for low-work-function surfaces. On the other hand, at small exit angles, the neutralization mainly takes place in region III (large distances) where the large neutral fraction is favored by the long interaction time. In the case of Cu(110), the calculated results follow the trend of the experimental data at small exit angles, but it fails for the cases of Au(111), Pd(111), and Cu(111) due to negligible energy width for neutralization in region II or III. In addition, in Fig. 6 the exit angle corresponding to the minimum of neutral fraction shifts from ∼40° to ∼22° with the increase of surface work function, which further indicates that the neutralization at short distances gradually dominates for high-work-function surfaces. This is similar to the case of the exit velocity dependence.

Considering the parallel velocity effect, the calculated neutral fraction increases significantly at small exit angles in Figs. 10(a)–10(c), since small exit angle corresponds to high parallel velocity for a given incident energy. For high-work-function surfaces, the parallel velocity enhances the neutralization, corresponding to decreasing the surface work function or increasing the binding energy of the projectile.

At present, the model cannot resolve the neutralization at large distances for high-work-function surfaces. Therefore the calculation cannot reproduce the trend at low perpendicular exit velocity or that at low exit angle. Note that, compared with (111) faces, the nonmonotonic exit energy and angle dependences have also been observed in the previous studies on the neutralization of Li^+ ions scattering on Au(110) and Pd(100) surfaces [33] and in this work for Na^+ ions scattering on Cu(110), which is independent of the differences in details of the electronic structure of these surfaces. In general, the calculated results are not in quantitative agreement with experiment. First, the *L*-band gap is a characteristic of all the (111) faces of noble metals. For (111) faces, the calculated results are lower than the data, since in our calculation the jelliumlike energy-level width is used and does not consider the realistic electronic structure of the (111) surfaces. At short distances, the Na(3*s*) state lies below the band gap, and it is in resonance with the valence band of the surface. As the ion-surface distance increases, the presence of the *L*-band gap should lead to a strong decrease in electron loss from the populated Na(3*s*) level to the conduction band of the (111)

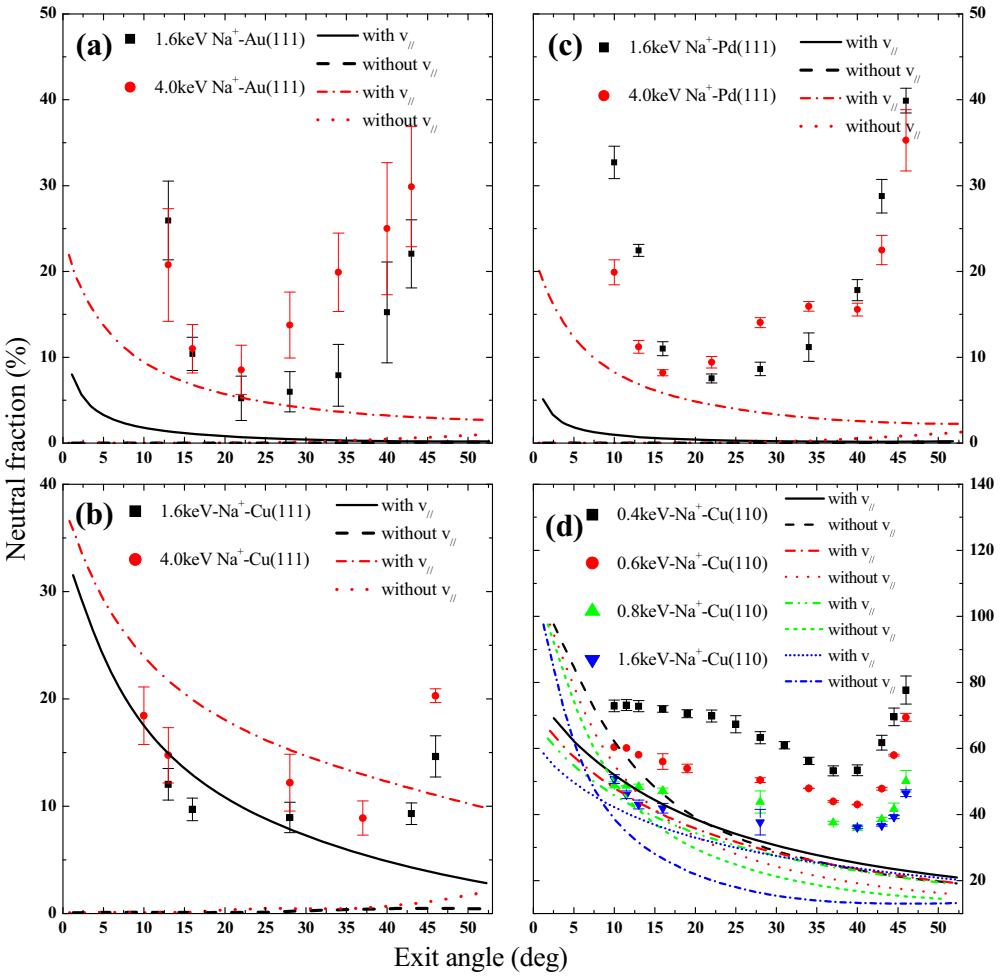

FIG. 10. Calculated neutral fractions as a function of exit angle are compared with the experimental data from Fig. 6 for 1.6-keV (■) and 4-keV (●) Na^+ scattering on (a) Au(111), (b) Cu(111), (c) Pd(111), and (d) Au(111) surfaces with a scattering angle of 53.

face [32,33]. Second, for the (111) faces, the surface states are close to the bottom edge of the band gap, which may affect the neutralization process via quasiresonant electron capture from the surface states [32]. Compared with Au(111) and Cu(111), the first image state in Pd(111) is located almost at the center of the band gap. The image state may enhance the neutralization rate, which has been reported for the case of Li ion scattering [35]. Third, in the model the position and the width of the Na(3*s*) level are approximately obtained from the literature. This may introduce the difference between calculation and experiment.

It is important to remark that some efforts have been devoted to the unknown physical mechanism of efficient neutralization at large distances for high-work-function surfaces. First, the inclusion of a large number of surface atoms is essential to change the energy-level width at large ion-surface distances and increase the neutral fraction in the low-energy range [37]. Second, the correct inclusion of electronic structure of surfaces (i.e., surface states, image states [35], and band gaps [48,61]), might improve the theoretical description. At last, the multiple collision events [62], related to the trajectory effect [33], should also be taken into account for efficient neutralization at much low velocities.

V. CONCLUSIONS

In this work, we have presented data of Na^+ neutralization on Au(111), Pd(111), Cu(111), and Cu(110). This work has improved significantly on our previous work in four aspects. First, the angle-dependent neutralization has been systematically measured for these four surfaces. Second, we have used a small scattering angle of 7° to compare with the results from large scattering angles. Third, we have extended the incident energy to 5 keV. Fourth, we have provided a quantum-mechanical method to describe the dynamical neutralization process, which is kept rather simple and easy to handle.

For high-work-function surfaces like Au(111) and Pd(111), efficient neutralization has been surprisingly observed. For these four surfaces, the neutral fraction decreases with the increase of the work function. With the increase of surface work function, the nonmonotonic energy dependence of the neutral fraction becomes more and more obvious in the extended energy range investigated. For Cu(111) and Cu(110) at the scattering angle of 7°, the energy dependence of the neutral fraction is still nonmonotonic as compared to the scattering angles of 135° and 53°. Compared to Au(111) and Pd(111), Cu(110) with lower work function still has the

nonmonotonic angle dependence of the neutral fraction, which indicates that the dynamic neutralization at short distances can be well studied via measuring the exit angle dependence. Moreover, the competition between neutralization at short distances and at large distances strongly depends on the surface work function.

The neutralization cannot be completely understood by the jellium model. Our calculations based on the well-known BN model clearly delineate the dynamical electron transfer features in alkali-metal ion neutralization. The essences of the nonmonotonic energy and angle dependences are the same, in spite of the differences in details of the surface work function and electronic structure of these surfaces. The atomic level shifts down below the Fermi level at short distances (region I), which causes high neutralization probability dominating at relatively large exit energies, while the neutralization at large distances (region III) dominates at lower exit energies. The neutralization may be enhanced by the relatively large parallel velocity. The parallel velocity effect corresponds to the reduced work function or the increased binding energy of the projectile which leads to the increase of the crossing distance between the Fermi level and the atomic level (region I). Thus the neutralization affected by the parallel velocity effect is significant at large exit energies or at low exit angle, as shown in Figs. 9 and 10.

Note that the modified BN model can reproduce the nonmonotonic neutral fraction trend for Cu(110); however, it fails in the case of high-work-function surfaces because at present we have not found a reasonable mechanism responsible for efficient neutralization at large distances where the atomic level may be above the Fermi level of the surface. Therefore we expect that this work will stimulate further theoretical study on this subject.

ACKNOWLEDGMENTS

The authors gratefully acknowledge J. D. Fuhr and M. L. Martiarena for helpful discussion. The authors are grateful to J. J. Lu, H. Y. Jiang, and W. B. Wu for their help in the initial stages of the experiment. This work is supported by the National Natural Science Foundation of China (Grants No. 11474140 and No. 11405078), the Fundamental Research Funds for the Central Universities (Grant No. lzujbky-2017-it41), and the National Students' Innovation and Entrepreneurship Training Program (Grants No. 201410730069 and No. 201510730078).

[1] J. A. Gibbard, M. Dethlefsen, M. Kohlhoff, C. J. Rennick, E. So, M. Ford, and T. P. Softley, Phys. Rev. Lett. **115**, 093201 (2015).
[2] I. K. Gainullin and M. A. Sonkin, Phys. Rev. A **92**, 022710 (2015).
[3] M. Pamperin, F. X. Bronold, and H. Fehske, Phys. Rev. B **91**, 035440 (2015).
[4] A. Iglesias-García, F. Bonetto, R. Vidal, J. Ferrón, and E. C. Goldberg, Phys. Rev. A **89**, 042702 (2014).
[5] X. He and J. A. Yarmoff, Phys. Rev. Lett. **105**, 176806 (2010).
[6] A. Schmitz, J. Shaw, H. S. Chakraborty, and U. Thumm, Phys. Rev. A **81**, 042901 (2010).
[7] R. C. Monreal, Prog. Surf. Sci. **89**80 (2014); C. L. Moss, C. M. Isborn, and X. Li, Phys. Rev. A **80**, 024503 (2009).
[8] L. Chen, B. Ding, Y. Li, S. L. Qiu, F. F. Xiong, H. Zhou, Y. L. Guo and X. M. Chen, Phys. Rev. A **88**, 044901 (2013); A. G. Borisov and V. A. Esaulov, J. Phys.: Condens Matter **12R**, 177 (2000).
[9] M. Wiatrowski, L. Lavagnino, and V. A. Esaulov, Surf. Sci. **601**, L39 (2007).
[10] J. P Gauyacq, A. G. Borisov, and D. Teillet-Billy, in *Formation/Destruction of Negative Ions in Heavy Particle-Surface Collisions*, edited by V. A. Esaulov (Cambridge University Press, Cambridge, UK, 1996).
[11] U. Heiz and W.-D. Schneider, J. Phys. D: Appl. Phys. **33**, R85 (2000).
[12] J. Lee, Z. Zhang, and J. T. Yates, Jr., Phys. Rev. B **79**, 081408 (2009).
[13] A. M. Belu, D. J. Graham, and D. G. Castner, Biomaterials **24**, 3635 (2003).
[14] H. H. Brongersma, M. Draxler, M. de Ridder, and P. Bauer, Surf. Sci. Rep. **62**, 63 (2007).
[15] M. P. Ray, R. E. Lake, C. E. Sosolik, L. B. Thomsen, G. Nielsen, I. Chorkendorff, and O. Hansen, Phys. Rev. B **80**, 161405 (2009).
[16] M. P. Ray, R. E. Lake, L. B. Thomsen, G. Nielson, O. Hansen, I. Chorkendorff, and C. E. Sosolik, J. Phys.: Condens. Matter **22**, 084010 (2010).
[17] J. A. Yarmoff, Y. Yang, and Z. Sroubek, Phys. Rev. Lett. **91**, 086104 (2003).
[18] Y. Yang and J. A. Yarmoff, Surf. Sci. **573**, 335 (2004).
[19] Y. Yang, Z. Sroubek, and J. A. Yarmoff, Phys. Rev. B **69**, 045420 (2004).
[20] G. F. Liu, P. Karmakar, and J. A. Yarmoff, Phys. Rev. Lett. **98**, 176104 (2007).
[21] A. R. Canário and V. A. Esaulov, J. Chem. Phys. **124**, 224710 (2006).
[22] J. Shen, J. Jia, K. Bobrov, L. Guillemot, and V. A. Esaulov, J. Phys. Chem. C **119**, 15168 (2015).
[23] G. F. Liu, Z. Sroubek, and J. A. Yarmoff, Phys. Rev. Lett. **92**, 216801 (2004).
[24] H. Hövel and I. Barke, New J. Phys. **5**, 31 (2003).
[25] N. Nilius, M. Kulawik, H.-P. Rust, and H.-J. Freund, Surf. Sci. **572**, 347 (2004).
[26] M. Valden, X. Lai, and D. W. Goodman, Science, **281**, 1647 (1998).
[27] I. K. Gainullin, E. Yu. Usman, Y. W. Song, and I. F. Urazgildin, Vacuum **72**, 263 (2003).
[28] E. Y. Usman, I. F. Urazgil'din, A. G. Borisov, and J. P. Gauyacq, Phys. Rev. B **64**, 205405 (2001).
[29] E. V. Chulkov, V. M. Silkin, and P. M. Echenique, Surf. Sci. **437**, 330 (1999).
[30] T. Kravchuk, Yu. Bandourine, A. Hoffman, and V. A. Esaulov, Surf. Sci. **600**, L265 (2006).
[31] A. R. Canário, A. G. Borisov, J. P. Gauyacq, and V. A. Esaulov, Phys. Rev. B **71**, 121401 (2005).
[32] A. R. Canário, T. Kravchuk, and V. A. Esaulov, New J. Phys. **8**, 227 (2006).

[33] L. Chen, J. Shen, J. Jia, T. Kandasamy, K. Bobrov, L. Guillemot, J. D. Fuhr, M. L. Martiarena, and V. A. Esaulov, Phys. Rev. A **84**, 052901 (2011).
[34] H. Hamoudi, C. Dablemont, and V. A. Esaulov, Surf. Sci. **602**, 2486 (2008).
[35] F. J. Bonetto, E. A. García, C. González, and E. C. Goldberg, J. Phys. Chem. C **118**, 8359(2014).
[36] E. A. García, M. A. Romero, C. González, and E. C. Goldberg, Surf. Sci. **603**, 597 (2009).
[37] C. Meyer, F. Bonetto, R. Vidal, E. A. Garcia, C. Gonzalez, J. Ferrón, and E. C. Goldberg, Phys. Rev. A **86**, 032901 (2012).
[38] I. K. Gainullin, Phys. Rev. A **95**, 052705 (2017).
[39] P. Y. Liu, L. Chen, S. L. Qiu, F. F. Xiong, H. Y. Jiang, J. J. Lu, Y. F. Liu, G. P. Li, Y. R. Liu, F. Ren, Y. Q. Xiao, L. Gao, B. Ding, Y. L. Guo, and X. M. Chen, J. Phys. Chem. C **120**, 18538 (2016).
[40] R. S. Gao, P. S. Gibner, J. H. Newman, K. A. Smith, and R. F. Stebbings, Rev. Sci. Instrum. **55**, 1756 (1984).
[41] H. C. Straub, M. A. Mangan, B. G. Lindsay, K. A. Smith, and R. F. Stebbings, Rev. Sci. Instrum. **70**, 4238 (1999).
[42] N. Takahashi, Y. Adachi, M. Saito, and Y. Haruyama, Nucl. Instrum. Methods Phys. Res., Sect. B **315**, 51 (2013).
[43] MPA-3, FAST ComTec. See the production information at: https://www.fastcomtec.com/products/mca/#.
[44] Q. Wang, S. Qiu, F. Xiong, Y. Li, B. Ding, Y. Guo, X. Chen, and L. Chen, Eur. Phys. J. D **69**, 210 (2015).
[45] L. Chen, S. Qiu, F. Xiong, J. Lu, P. Liu, B. Ding, Y. Li, Y. Cui, Y. Guo, and X. Chen, J. Chem. Phys. **143**, 114703 (2015).
[46] M. P. Ray, R. E. Lake, J. B. Marston, and C. E. Sosolik, Surf. Sci. **635**, 37 (2015).
[47] G. A. Kimmel and B. H. Cooper, Phys. Rev. B **48**, 12164 (1993).
[48] A. G. Borisov, J. P. Gauyacq, E. V. Chulkov, V. M. Silkin, and P. M. Echenique, Phys. Rev. B **65**, 235434 (2002).
[49] A. G. Borisov, G. E. Makhmetov, D. Teillet-Billy, and J. P. Gauyacq, Surf. Sci. **375**, L367 (1996); A. G. Borisov, A. K. Kazansky, and J. P. Gauyacq, Phys. Rev. B **59**, 10935 (1999).
[50] A. V. Onufriev and J. B. Marston, Phys. Rev. B **53**, 13340 (1996).
[51] R. Brako and D. M. Newns, Surf. Sci. **108**, 253 (1981).
[52] L. Chen, W. B. Wu, P. Y. Liu, Y. Q. Xiao, G. P. Li, Y. R. Liu, H. Y. Jiang, Y. L. Guo, and X. M. Chen, Chin. Phys. B **25**, 083401 (2016).
[53] P. Nordlander and J. C. Tully, Phys. Rev. B **42**, 5564 (1990).
[54] F. Bonetto, M. A. Romero, E. A. García, R. A. Vidal, J. Ferrón, and E. C. Goldberg, Phys. Rev. B **78**, 075422 (2008).
[55] A. G. Borisov, D. Teillet-Billy, J. P. Gauyacq, H. Winter and G. Dierkes, Phys. Rev. B **54**, 17166 (1996).
[56] R. D. Gann, J. X. Cao, R. Q. Wu, Jinsheng Wen, Zhijun Xu, G. D. Gu, and J. A. Yarmoff, Phys. Rev. B **81**, 035418 (2010).
[57] G.F. Liu, J. A. Yarmoff, Surf. Sci. **600**, 2293 (2006).
[58] H. Winter, Phys. Rep. **367**, 387 (2002).
[59] A. G. Borisov, D. Teillet-Billy, J. P. Gauyacq, J. A. M. C. Silva, A. Mertens, C. Auth, and H. Winter, Phys. Rev. B **59**, 8218 (1999).
[60] T. Hecht, H. Winter, A. G. Borisov, J. P. Gauyacq, and A. K. Kazansky, Phys. Rev. Lett. **84**, 2517 (2000).
[61] K. Niedfeldt, E. A. Carter, and P. Nordlander, Surf. Sci. **600**, L291 (2006).
[62] A. Sindona, M. Pisarra, S. Maletta, P. Riccardi, and G. Falcone, J. Phys.: Condens. Matter **22**, 475004 (2010).